P3.2

A MACHINE INTELLIGENT GUST FRONT ALGORITHM FOR DOPPLER WEATHER RADARS

Richard L. Delanoy and Seth W. Troxel

MIT Lincoln Laboratory
Lexington, Massachusetts

1. INTRODUCTION

Gust fronts exist at the leading edge of cold air outflows from thunderstorms. The outflows, which are deflected horizontally at the ground, may propagate many miles ahead of the generating thunderstorm. Since they often produce pronounced changes in wind speed and direction, gust fronts can have a significant impact on air terminal operations by forcing a change of active runway and a rerouting of aircraft already in the terminal area. Consequently, for reasons of aviation safety and airport operations efficiency, gust front detection and tracking is an important product of Doppler weather radars developed for use in airport terminal areas.

Systems developed for the task of airport weather surveillance include the Terminal Doppler Weather Radar (TDWR) and the Airport Surveillance Radar with Wind Shear Processor (ASR–9 WSP). In Doppler velocity images obtained from these radars, gust fronts are recognizable as boundaries between converging velocities. In reflectivity images, gust fronts appear as thin lines of increased intensity, which occur as the result of particulate scatterers being lofted and concentrated at the leading edge of the front.

Current generation algorithms, such as the Gust Front Detection Algorithm (GFDA; Witt 1987, Smith 1989, Hermes 1992) and the Advanced Gust Front Algorithm (AGFA; Merritt 1989, Eilts 1991), are based on an approach developed nearly 10 years ago (Uyeda 1986). This approach attempts to detect one or both signatures relying on techniques characterized by 1–dimensional (radially aligned) signal processing, sequential thresholding of data, and complicated *ad hoc* heuristics. These algorithms work well when the gust front signatures are clear and unambiguous; respectable levels of performance have been achieved by these algorithms when applied to TDWR images. However, weak or ambiguous signatures can easily be missed or confused with other weather phenomena. For example, convergence signatures disappear as gust fronts become radially aligned. Also, reflectivity thin lines can be obscured by low altitude precipitation or may be difficult to detect in clear, dry air. Finally, convergence and thin line signatures can arise from phenomena unassociated with gust fronts.

Corresponding author address: Richard L. Delanoy, 244 Wood Street, MIT Lincoln Laboratory, Lexington, MA 02173–9108

*The work described here was sponsored by the Federal Aviation Administration. The United States Government assumes no liability for its content or use thereof.

The ASR–9 WSP provides a less expensive alternative to the pencil–beam, high resolution TDWR (Weber 1989). Although not originally intended for weather imaging, the ASR–9 WSP generates images of sufficient quality that gust fronts can be identified and tracked by human interpreters. However, versions of AGFA adapted for ASR–9 WSP data have performed poorly. The lack of performance is due primarily to the reduced gain and lowered sensitivity inherent in the fan–beam design of the ASR–9. With lowered sensitivity, clear air velocity estimates are unreliable, making most convergence signatures invisible. Consequently, AGFA is forced to rely on only the thin–line portion of the algorithm. To make matters worse, the reduced sensitivity also makes faint thin–line signatures more fragmented and harder to resolve from background.

Since humans can discriminate gust fronts much better than the existing algorithms given the same Doppler weather radar images, there is apparently information available in the images that is not being effectively exploited. Some possibilities include the more effective use of weak signatures, motion, spatial and environmental context, and multiple sources of evidence.

Machine intelligence techniques, originally developed at Lincoln Laboratory in the context of automatic target recognition, provide more effective means for exploiting, organizing, and assimilating such additional information (Verly 1989, Delanoy 1992a, Delanoy 1992b, Delanoy 1993a). These approaches to object recognition have been used to construct a Machine Intelligent Gust Front Algorithm (MIGFA) that is radically different from previous gust front detection algorithms. Versions of MIGFA have been developed for application to both ASR–9 WSP and TDWR images. Evaluations made thus far indicate that MIGFA substantially outperforms earlier approaches and may be competitive with human observers.

Given that the ASR–9 WSP version was developed first, has undergone operational testing and evaluation, and represents the harder technical challenge, we will present the ASR–9 WSP version of MIGFA in this paper. A detailed description of MIGFA and the concepts and techniques of low–level machine intelligence can be found in Delanoy 1993b and Delanoy 1993c.

2. LOW–LEVEL MACHINE INTELLIGENCE

The conventional wisdom in computer vision/object recognition research has been to use general image processing operations, ideally devoid of object– and context–dependent knowledge, at the initial stages of processing. Such operations might include edge detection, segmentation, cleaning, or optic flow estimations. From the results of such general operations, image characteristics are extracted and represented symbolical-

ly. Machine intelligence is then applied, as if by definition, only on the symbolic representations at "higher" levels of processing. In contrast, sensor–, object–, and context–dependent knowledge is applied in the earliest (image processing) levels of XTRS and MIGFA processing through the use of two techniques.

2.1. Functional Template Correlation

The first technique, functional template correlation (FTC) (Delanoy 1992a) is a generalized matched filter incorporating aspects of fuzzy set theory. For comparison, standard 2–D cross correlation relies upon a kernel that is essentially a sub–image consisting of expected image values. In contrast, the kernel of a functional template consists of a set of integers that each correspond to a unique scoring function. Each scoring function, given an image value as input, returns a score reflecting how well that image value matched expectations for a given location on the kernel. The results of all scoring functions within the functional template are then averaged, resulting in an overall match score in the range [0,1]. The output of FTC is a map of these values, each of which reflects the degree of belief that the shape or object implicitly encoded in a functional template is present at that image location.

As an example, consider the functional template implementation of a simple matched filter shown in Figure 1, which is designed to detect gust fronts in reflectivity data. Gust fronts are observed as thin lines of moderate reflectivity (approximately 0 to 20 dBZ), that are flanked on both sides by low reflectivity values (approximately –10 to 0 dBZ). On the left is the template kernel consisting of integers, corresponding to the two scoring functions shown on the right. Elements of the kernel that do not have an index form guard regions in which image values are ignored and have no effect on match scores. Scoring function 0, corresponding to the flanking regions of low reflectivity, returns a maximal score of 1.0 for image values in the interval of –20 dBZ to –5 dBZ, a gradually decreasing score for image values in the interval –5 dBZ to 10 dBZ, and a score of –2.0 for image values larger than 10 dBZ. Scoring function 1, corresponding to the center of the kernel where moderate reflectivity values are expected, returns maximal scores in the interval between 5 and 12.5 dBZ.

By increasing or decreasing the interval over which affirming scores (i.e., > 0.5) are returned, scoring functions can encode varying degrees of uncertainty with regard to what image values are allowable. But in addition, knowledge of how a feature or object appears in sensor imagery can be encoded in scoring functions. With various design strategies, the interfering effects of occlusion, distortion, noise, and clutter can be minimized. As a consequence, matched filters customized for specific applications using FTC are generally more robust than standard signal processing operations.

2.2. Interest Images

Knowledge of the varying reliability of the selected feature detectors is used to guide data fusion. Such conditional data fusion is simplified by using "interest" as a common denominator (Delanoy 1993b). An interest image is a map of numeric values in the range [0,1], indicating the presence of some feature that is selectively indicative of an object being sought (the output of FTC is an interest image as long as the functional template encodes an indicative feature). Higher pixel values reflect greater confidence that the intended feature is present at that location. Clusters of high values in the combined interest image are then used to guide selective attention and serve as the input for object extraction. Because interest values are dimensionless and given the assumption that the output of any feature detector can be configured as an interest image, evidence from any number of registered sources of information can be easily combined using simple or arbitrarily complex rules of arithmetic or fuzzy logic.

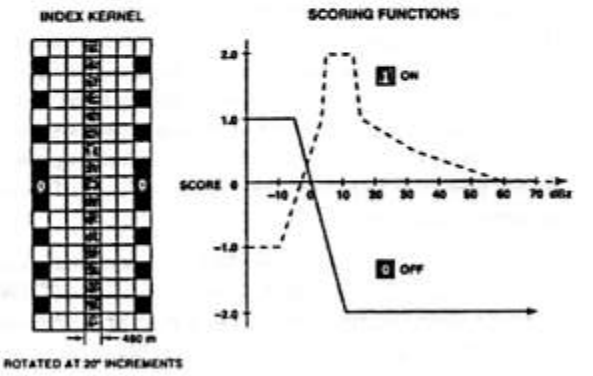

Figure 1. Example functional template for thin line feature detection.

An individual feature detector may be reliable only under certain identifiable circumstances. By using knowledge of such circumstances and by allowing feature detectors to mutually support or compensate for each other, relatively good performance can be achieved using feature detectors that may individually be weakly or inconsistently discriminating. If done effectively, the combined interest image provides a better representation of object shape than is evident in any single sensory modality.

3. ALGORITHM DESIGN

The system block diagram in Figure 2 illustrates the configuration of the ASR–9 WSP version of MIGFA described below.

3.1. Input Images

Reflectivity and velocity data are converted from polar to Cartesian format, producing images DZ (reflectivity image) and V (Doppler velocity image), respectively. As part of the conversion to Cartesian format, the data are subsampled so that the pixel size is 480 meters per pixel.

Although convergence signatures are not reliably visible in ASR–9 data, the velocity data does contain relevant information. Velocity measurements within a gust front thin line region have higher signal–to–noise ratios, and consequently lower local Doppler variance, than the surrounding clear air measure-

ments. Therefore, a map of velocity local standard deviation (SD) is computed from V. Gust fronts appear in SD as thin lines of low variance against a background of high variance.

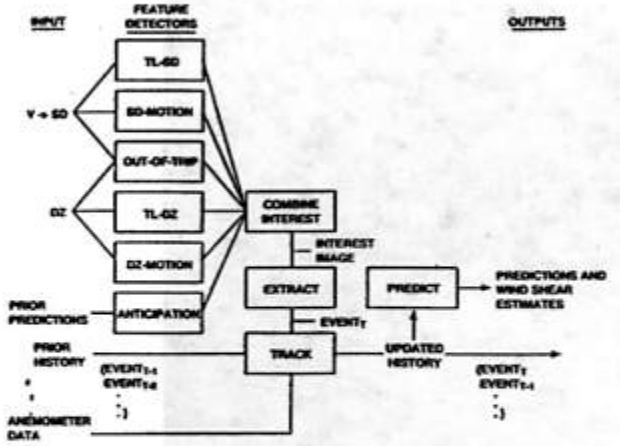

Figure 2. MIGFA block diagram.

3.2. Feature Detectors

Feature detector TL–DZ in Figure 2 applies the thin line filter shown in Figure 1 to the reflectivity image DZ. The output is an interest image highlighting with high pixel values locations where thin lines are found in DZ. The second feature detector, DZ–MOTION, applies a similar thin line filter to the difference of two sequential DZ images. The thin line filter in DZ–MOTION uses the same kernel as TL–DZ, but utilizes scoring functions that reflect the effects of image differencing. Image differencing is used not only to eliminate thin lines that are not moving, but to suppress the background levels of reflectivity, improving the observability of thin lines. The feature detectors TL–SD and SD–MOTION use thin line filters similar to those used in TL–DZ and DZ–MOTION. They differ only in that the scoring functions are suited for values of Doppler standard deviation instead of reflectivity.

The feature detector OUT–OF–TRIP identifies range–ambiguous echoes of more distant weather. Thin lines highlighted in the TL–DZ and DZ–MOTION interest images that are radially aligned (+/– 10 degrees) and that coincide with high OUT–OF–TRIP interest values are suppressed.

The final feature detector, ANTICIPATION, provides a mechanism for spatially adjusting the detection sensitivity of MIGFA on the basis of knowledge of various environmental data, including the prior history of the gust fronts being tracked and dominant weather patterns. In particular, anticipation is used as a replacement for *coasting*, which is the continued tracking of an object on a radar screen for some time interval after the object signal falls below threshold. Coasting works only when the target being tracked maintains a consistent velocity. But in reality, the reason the object signal falls below threshold is often because the object did change behavior. In contrast, anticipation works by creating bands of high interest values where the object is expected to be in the current scan. Anticipation is set not so high as to trigger a detection by itself, but high enough to raise collocated weak signals above detection threshold.

3.3. Combining Interest

The interest images generated by the four feature detectors TL–DZ, TL–SD, DZ–MOTION, and SD–MOTION are averaged together (missing values are ignored). The resulting averaged interest image and the ANTICIPATION interest image are combined as a weighted average; ANTICIPATION is given a weight of 0.25 while the average of the first four interest images is given a weight of 0.75. The resulting image is the combined INTEREST image, an example of which is shown in Figure 3.

3.4. Extraction

The goal of extraction in MIGFA is to identify the set of points (collectively called an *event*) that lie in *any* gust front. Individual points are tracked across time; the fact that a point belongs to one gust front or another is irrelevant to processing. Because different points can have variable velocities, MIGFA predictions are elastic.

The thin line shapes evident in the combined interest image are smoothed, thresholded, and thinned, resulting in chains of points. The resulting chains are extended from their end points along ridges of relatively high interest values. At this point, the chains of points may form one or more disjoint complex networks, each potentially with internal closed loops and multiple end points. From each network of chain fragments is assembled the most interesting (typically, but not necessarily, the longest) combined chains of points. An example of extracted gust front points is shown in Figure 3.

3.5. Tracking and Prediction

Tracking is done by establishing point–by–point correspondence between successive scans. For each point in the current scan, a point in the previous scan is found that is nearby and that has a propagation velocity consistent with the point in the current scan. Once correspondence is established, a link is created from the point in the current scan to its corresponding point in the previous scan. After indexing is completed, each extracted chain of points is edited in order to smooth the computed propagation speeds and orientations over local segments of the chains. Heuristics are then used to verify the detections, making use of knowledge of how gust fronts move. Chains exhibiting patterns of motion that are improbable are rejected.

The current extracted event, indexed into the prior history, is used to make predictions of where the points having sufficient depth and interest are likely to be at some time in the future. Given the direction moved, the propagation speed, and the current coordinates of an extracted point, a new coordinate is computed for some time in the future. Figure 3F shows the 10 and 20 minute predictions for two colliding gust fronts.

Figure 3. Summary of the results of processing a ASR–9 WSP scan containing two colliding gust fronts. (A) The reflectivity image DZ. (B) The image of local Doppler standard deviation SD. (C) The combined INTEREST image. (D) The set of extracted points called an EVENT. (E) The gust front points shown in the context of prior HISTORY. (F) The 10 and 20 minute PREDICTIONS of gust front location.

4. RESULTS

A test set of ASR–9 WSP data collected in Orlando, Florida during AGFA field testing in 1991 contains 9 different gust fronts in a set of 450 images (15 hours). A human interpreter looking at the same ASR–9 WSP data detected 280 instances of these 9 gust fronts. Four figures of merit are shown for each of the two systems. The probability of detection is the number of detections made by each algorithm as a percent of human detected instances of gust fronts. The probability of false alarm (PFA) is the number of false alarms divided by the total number of detections. In addition to simply identifying fronts, the human interpreter delimited the length of each detected front. Detection quality was further assessed by comparing the length of the front as estimated by each algorithm and the human interpreter. The percent length detected (PLD) is the length detected expressed as a percent of the length delimited by the human interpreter. The percent of false length detected (PFD) reflects situations where the detected gust front lengths extended beyond what the human interpreter could see.

This same version of MIGFA was installed on an ASR–9 WSP in Orlando, Florida for operational testing during the summer of 1992, results of which are shown in Table 3. During the period from 1 August to 20 September, MIGFA correctly detected and tracked approximately 75% of all gust fronts identified by human interpreters examining ASR–9 WSP data. TDWR and anemometer data were also used for verification. Those gust fronts that were missed either had reflectivity levels near the sensitivity limits of the ASR–9 or were obscured by storm cells along the front.

Table 1. AGFA and MIGFA performance on ASR–9 WSP data as scored against human interpretations.

	Gust Fronts		Gust Front Length	
	POD	PFA	PLD	PFD
AGFA	56.7	4.6	38.9	12.9
MIGFA	88.1	0.6	86.2	33.4

Table 2. AGFA and MIGFA performance on ASR–9 WSP data as scored against human interpretations of matching TDWR data.

	Gust Fronts		Gust Front Length	
	POD	PFA	PLD	PFD
AGFA	42.6	3.2	21.0	4.2
MIGFA	75.1	0.0	58.7	6.4

Table 3. Results of MIGFA operational testing on ASR–9 WSP data collected in Orlando during summer 1992.

	Gust Fronts		Gust Front Length	
	POD	PFA	PLD	PFD
MIGFA	75.4	1.8	80.8	21.1

The false alarm rate (PFA) of 1.8% represents 19 false alarms out of 14000 scans processed. Most of these were short lived and all were too far from the airport to affect airport operations. The relatively high PFD score (21%) would seem to suggest that MIGFA has a problem discriminating the ends of gust fronts from clutter. Although a complete set of TDWR–based truth has not yet been compiled for these data, an analysis of individual cases again agrees with the offline evaluation (e.g., Tables 1 and 2) that the relatively high PFD consists largely of believable extensions of gust fronts that the human interpreter missed.

5. CONCLUSIONS

Detectors for thin–line convergence signatures in Doppler radar images are conceptually easy to define and implement in automated detection algorithms. And yet, despite the combined efforts of several research groups working for nearly 10 years to develop reliable automatic gust front algorithms, no algorithm has demonstrated capabilities comparable to the ideal of human performance.

The problem is that automatic gust front detection is deceptively a much harder problem than simply detecting one or both of these signatures. In order for human interpreters to detect and track gust fronts, they make use of knowledge about the radar and the weather. They use spatial and temporal context. And, they have the ability to deal with uncertainty while assimilating ambiguous or even contradictory evidence. The large performance gap between the performance of previous algorithmic approaches and humans in detecting gust fronts is in part due the lack of these perceptual skills. These deficiencies are addressed in MIGFA through the use of interest images as a mechanism for fusing evidence at the pixel level, 2–D signal processing (spatial context), motion (temporal context), fuzzy set theory (embodied in the use of functional template correlation and interest images), and delayed thresholding.

During the summer of 1993 operational testing of MIGFA will be done in Albuquerque, NM with the ASR–9 WSP version and in Orlando, FL for the TDWR version. MIGFA is currently the prime candidate for deployment in production ASR–9 WSP systems and may well be retrofitted to production TDWR's. Adaptations of the techniques used in MIGFA are currently being used, or are being considered, for other weather detection problems, including microburst prediction (Wolfson, 1993), convective storm initiation, and sensor fusion.

REFERENCES

Delanoy, R.L., J.G. Verly, and D.E. Dudgeon, 1992(a): Functional templates and their application to 3–D object recognition, *Proceedings of the 1992 International Conference of Acoustics, Speech, and Signal Processing*, San Francisco, CA, March 23–26, 1992.

Delanoy, R.L., J.G. Verly, and B. Williams, 1992(b): Region–based target recognition from laser radar imagery using appearance models, Technical Report TR–933, MIT Lincoln Laboratory, Lexington, MA, July, 1992.

Delanoy, R.L., J.G. Verly, and D.E. Dudgeon, 1993(a): Pixel–level fusion using interest images, Technical Report TR–979, MIT Lincoln Laboratory, Lexington, MA, May 1993.

Delanoy, R.L. and S.W. Troxel, 1993(b): The machine intelligent gust front algorithm, Technical Report ATC–169, MIT Lincoln Laboratory, Lexington, MA, May 1993.

Delanoy, R.L. and S.W. Troxel, 1993(c): Machine intelligent gust front detection, *Lincoln Laboratory Journal*, Vol. 6, No. 1.

Eilts, M.D, S. Olson, G. Stumpf, L. Hermes, A. Abrevaya, J. Culbert, K. Thomas, K. Hondl, and D. Klingle–Wilson, 1991: An improved gust front detection algorithm for the TDWR, *Preprints, 4th International Conference on Aviation Weather Systems*, Paris, France, June 24–26, 1991, J37–J42.

Hermes, L., A. Witt, S. Smith, D. Klingle–Wilson, D. Morris, G. Stumpf, and M. Eilts: The gust front detection and wind shift algorithms for the Terminal Doppler Weather Radar system, *J. Atmos. Oceanic Tech.*, (in press), 1993.

Smith, S., A. Witt, M. Eilts, D. Klingle–Wilson, S. Olson, and J.P. Sanford: Gust front detection algorithm for the Terminal Doppler Weather Radar part I: current status, *Preprints, 3rd International Conference on the Aviation Weather System*, Anaheim, CA, January, 1989, 31–34.

Merritt, M. W., D. Klingle–Wilson, and S.D. Campbell, 1989: Wind Shear Detection with Pencil–Beam Radars, *Lincoln Laboratory Journal*, Vol. 2, No.3, 483–510.

Uyeda, H. and D. Zrnic, 1986: Automatic detection of gust fronts, *J. Atmos. Oceanic Tech.*, 3, 36–50.

Verly, J.G., R.L. Delanoy, and D.E. Dudgeon, 1989: Machine intelligence technology for automatic target recognition, *Lincoln Laboratory Journal*, Vol. 2, No. 2, 277–311.

Weber, M.E. and T.A. Noyes, 1989: Wind shear detection with airport surveillance radars, *Lincoln Laboratory Journal*, Vol. 2, No. 3, 511–526.

Witt, A. and S. Smith, 1987: Development and testing of the gust front algorithm. Technical Report DOT/FAA/PS–87/4, FAA, 1987.

Wolfson, M.M, R.L. Delanoy, M.C. Liepins, B.E. Forman, and R.G. Hallowell, 1993: The ITWS microburst prediction algorithm, *Preprints, 5th Conference on Aviation Weather Systems*, Vienna, VA, August 1993.